Structural, Morphological, and Spectroscopic Study of Zn doped Bi_{1.5}Nb_{1.5}CuO₇ Pyrochlore Compounds

Abba Malika¹, Abdesselem Noura², Menasra Hayet³, Benbrika Chaima⁴, Necira Zelikha⁵Gherib Safa⁶, Bouchtob Nadjette⁷

¹ University of Biskra, BP 145 RP, Biskra 07000, Departement of Science of Matter, Laboratory of Molecular Chemistry and Environment (Algeria).

^{2,4,5}University of Biskra, BP 145 RP, Biskra 07000, Departement of Science of Matter, Laboratory of Applied Chemistry (Algeria).

³University of Biskra, BP 145 RP, Biskra 07000, Departement of of Industrial Chemistry, Laboratory of Applied Chemistry (Algeria).

^{6,7}University of Biskra, BP 145 RP, Biskra 07000, Departement of Science of Matter, (Algeria).

The Author's Email:m.abba@univ-biskra.dz¹, noura.abdessalem@univ-biskra.dz², h.menasra@univ-biskra.dz³, chaima.benbrika@univ-biskra.dz⁴, z.necira@univ-biskra.dz⁵, bochtobegherib@gmail.com^{6,7}.

Received: 07/2023 Published: 10/2023

Abstract

In this study, we synthesized and characterized pyrochlore solid solutions, specifically Bi_{1.5}Nb_{1.5}Zn_xCu_{1-x}O₇(with x values of 0, 0.2, 0.6, 0.8, and 1), for their potential use as catalysts in the degradation of organic pollutants. These pyrochlore compositions were prepared using the solidsolid reaction technique and thoroughly characterized through X-ray diffraction, scanning electron microscopy, Fourier-transformInfrared and UV-vis spectroscopy. XRD analysis confirmed the presence of a cubic pyrochlore structure with Fd3m symmetry. Notably, we observed a consistent linear decrease in the lattice parameter as zinc concentration decreased, demonstrating the successful incorporation of zinc into the pyrochlore lattice. SEM observations revealed dense microstructures with limited intergranular porosity, indicative of structural integrity. Infrared spectroscopic analysis identified vibrations associated with metal-oxygen bonds, further confirming the pyrochlore nature of these compounds. Variations in absorption peak intensities were correlated with the substitution fraction x, primarily attributed to the differing masses of copper and zinc atoms. The energy band gap, determined via the Tauc-plot method, ranged from 2.72 eV (x = 0) to 3.35 eV (x = 1), consistently increasing. These findings underscore pyrochlore materials' potential as catalysts for environmental remediation, particularly in degrading organic pollutants.

Keywords:Pyrochlore; Bi_{1.5} Nb_{1.5}CuO₇; Cubic structure; Scherrer method; Band gap

Structural, Morphological, and Spectroscopic Study of Zn doped Bi_{1.5}Nb_{1.5}CuO₇ Pyrochlore Compounds

Tob Regul Sci. ™ 2023 ;9(2):193 - 206 DOI: doi.org/10.18001/TRS.9.2.13

1. Introduction

Recent scientific research has been significantly focused on materials with the pyrochlore structure, primarily due to their extraordinary diversity of properties [1]. These materials have gained prominence across various fields, from solid-state batteries to superconductors [2, 3] and photocatalysis [4-6].

Pyrochlores are known for their characteristic cubic structure, denoted as $A_2B_2O_7$, adopting a cubic crystal structure (Fd3m) having a lattice parameter 'a' of approximately 10 Å [7]. Their unique structure is composed of two types of cations, refered to as A and B. Remarkably, pyrochlores are renowned for their ability to accommodate a wide range of cations with varying valences (+3 and +4)[8], such as those from rare earth elements and transition metals. Examples of such pyrochlores include $Y_2Ti_2O_7[9], Y_2Mo_2O_7[10], Dy_2Ti_2O_7[6, 11], La_2Zr_2O_7[12, 13], and Bi_2Ru_2O_7[14], among others.$

Notably, pyrochlores can also be composed of three elements, namely A, B, and B', exhibiting different valences and following the general structure (AB')(B'B)O₇[15]. These compounds have been engineered to enhance various physical properties, including their superconducting behavior [16], metallic conductivity [17], and ionic conductivity[18].

The research undertaken by Caignaert Vincent et al. [19-21] has significantly contributed to the enhancement of pyrochlore properties by means of precise compositional adjustments. Employing the conventional solid-solid synthesis method, they adeptly engineered a diverse array of pyrochlore variants by amalgamating polyvalent cations. These efforts led to significant achievements, including substantial electrical conductivity in materials containing copper, exemplified in $Bi_{1.5}Sb_{1.5}Zn_{1-x}Cu_xO_7[20]$, and the observation of Curie-Weiss paramagnetic behavior. This paramagnetism featured a noteworthy Van Vleck contribution arising from the Sm^{+3} magnetic cation in $Bi_{1.5}$ - $xSm_xSb_{1.5}CuO_7[19]$.

Furthermore, the research conducted by Benhadria Naceur et al. [22] and Abdelbaky Mohamed et al. [23] underscored the significance of pyrochlore compounds and their diverse applications in fields such as the photocatalytic properties in the environment [24].

In our research, we synthesized pyrochlores with the formula Bi_{1.5}Nb_{1.5}Zn_xCu_{1-x}O₇, varying the zinc content (x) at values of 0, 0.2, 0.6, 0.8, and 1. To ensure the quality and purity of the synthesized products, we employed X-ray diffraction (XRD), Fourier-transform infrared spectroscopy (FTIR), scanning electron microscopy (SEM), and UV-visible spectroscopy to examine optical properties. It's worth noting that our synthesis method was based on the solid-state approach, and we carefully optimized our experimental conditions, drawing inspiration

Structural, Morphological, and Spectroscopic Study of Zn doped Bi_{1.5}Nb_{1.5}CuO₇ Pyrochlore Compounds

from prior research conducted by Hanene KORICHI[25], who used concentrations of 0, 0.25, 0.5, 0.75, and 1.

2. Experimental procedures

Pyrochlore $Bi_{1.5}Nb_{1.5}Zn_xCu_{1-x}O_7$ ceramics with $0 \le x \le 1$ were synthesized using a solid-solid process. Starting materials, which included Bi_2O_3 (99.9%, Aldrich), Nb_2O_5 (99.5%, Stream Chemicals), CuO (98%, Riedel-de Haen), and ZnO (99%, Biochem), were employed as the initial components. Our synthesis protocol involved a stepwise procedure with notable variations compared to the one utilized by Korichi Hanane[25].

In our method, the initial mixture was subjected to 2 hours of grinding, followed by the first calcination at 700°C (ramped at 2°C/min) for 24 hours. Subsequently, another 2-hour grinding cycle was performed, succeeded by calcinations at 800°C and 900°C, each under the same heating rate and time frame. The resulting material was shaped by pressing at a pressure of 3000 kg/cm², incorporating 5% polyvinyl, and underwent drying at 80°C. Finally, sintering was carried out at 920°C for a duration of 12 hours.

In contrast, Korichi Hanane's approach featured a different temperature profile and durations. Their initial mixture underwent grinding, followed by the initial calcination at 600°C (ramped at 2°C/min) for 24 hours. After an additional 2-hour grinding cycle, the material was subjected to calcinations at 700°C, 850°C, and eventually reached a final temperature of 900°C for 6 hours. The shaping process involved pressing at a pressure of 400 kgf/cm². Subsequently, the material underwent sintering at 920°C for an extended duration of 36 hours.

These variations in temperature profiles, calcination times, pressing pressures, and sintering durations likely contributed to differences in the final properties of the synthesized materials using the two protocols

The specimens were initially characterized using X-ray powder diffraction employing a Panalytical X'pert Pro X-ray diffraction system. Data collection was carried out using CuKa radiation through a step-scan method spanning the 2θ range from 10° to 80° . The step size was set at 0.016° , and each step had a duration of 0.5 seconds.

Microstructural analysis of the sintered samples was carried out using a scanning electron microscope (JEOL JSM 6390). The densities of the sintered samples were determined through the Archimedes method.

Fourier Transform Infrared spectroscopy (FTIR) of the samples was conducted using a PerkinElmer FT-IR Spectrum spectrophotometer, covering the wavelength range of 400–1500 cm⁻¹.

Structural, Morphological, and Spectroscopic Study of Zn doped Bi_{1.5}Nb_{1.5}CuO₇ Pyrochlore Compounds

The optical properties of all the samples were determined at room temperature in the 200-800 nm region using a UV-VIS spectrometer (Perkin Elmer Lambda 25 UV).

The steps followed in this synthesis protocol are illustrated in Fig. 1.

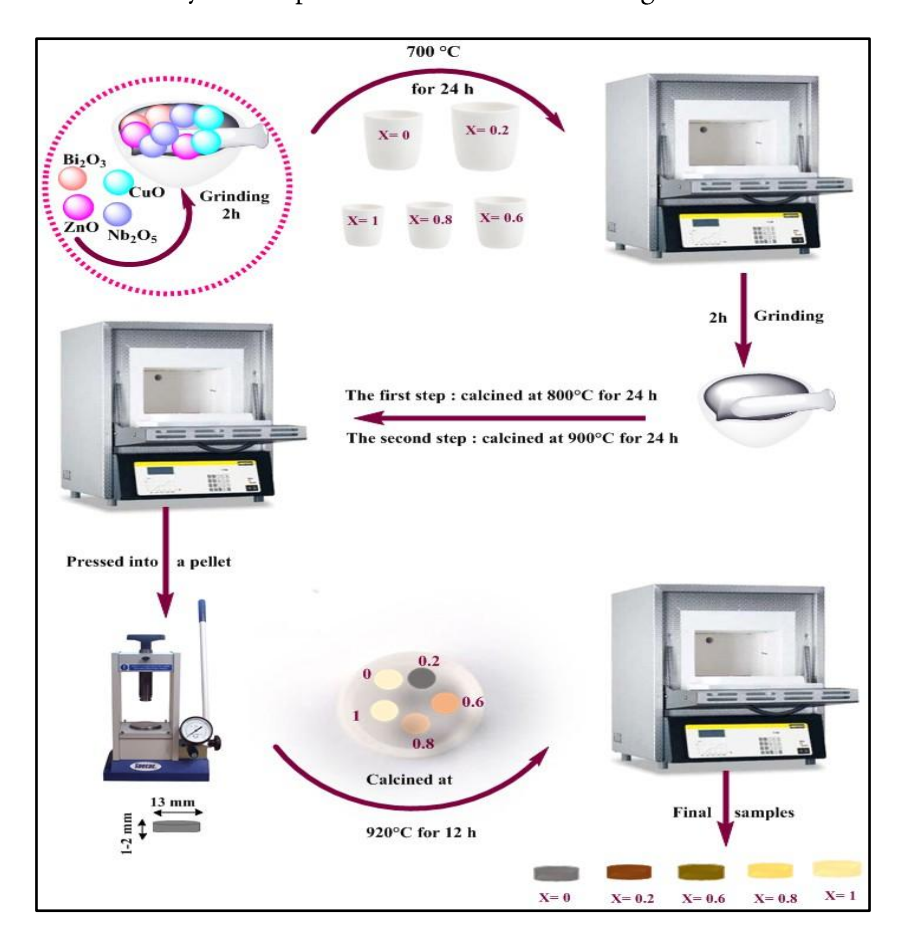


Fig. 1.Steps in Solid-State Preparation of Bi_{1.5}Nb_{1.5}Zn_xCu_{1-x}O₇Pyrochlore Samples

3. Results and discussions

3.1. X-ray Diffraction (XRD) Analysis

The substitution of copper with zinc led to the formation of a continuous solid solution of the pyrochlore type, characterized by the chemical formula $Bi_{1.5}Nb_{1.5}Zn_xCu_{1-x}O_7$, where x=0,0.2, 0.6, 0.8, and 1. Throughout the synthesis process for the different compositions, noteworthy color variations in the powder were observed, contingent on the temperature, as illustrated in Fig. 2.

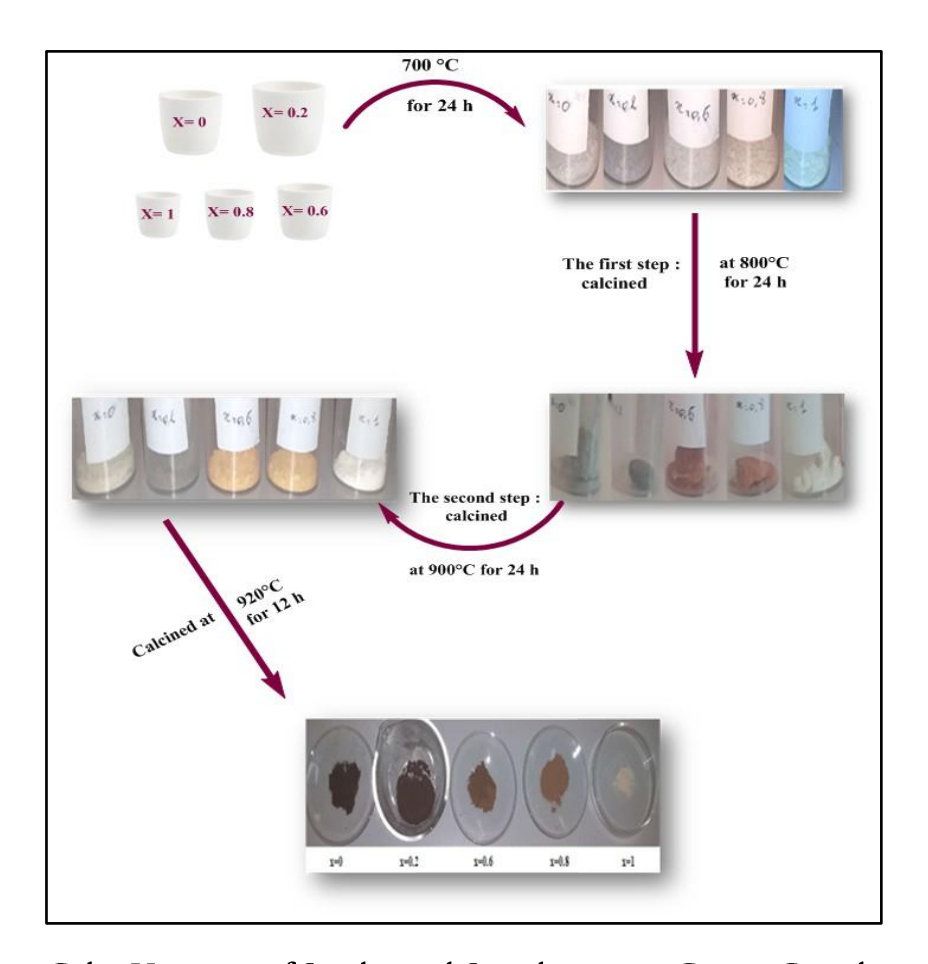


Fig. 2.Color Variation of Synthesized Samples at 700°C, 800°C, and 900°C.

The XRD pattern obtained, as illustrated in Fig. 3(a), reveals clear diffraction peaks corresponding to the cubic crystal structure of $Bi_{1.5}Nb_{1.5}ZnO_7$ (ICSD no. 00-054-0971) within the Fd3m space group. Specifically, the diffraction peaks for the (111), (311), (222), (400), (331), (511), (440), (622), (444), (800), and (622) planes of cubic Bi1.5Nb1.5ZnO7 were observed at 2θ angles of 14.51°, 28.04°, 29.31°, 33.97°, 37.13°, 44.61°, 48.79°, 57.94°, 60.78°,71.55° and 79.06°, respectively.

Fig. 3(b) offers an enlarged view of the XRD pattern within the angular range of (28.5°-30°), focusing specifically on the most intense diffraction peak (222). Notably, this peak consistently shifts toward lower angles (from29.40° to29.31°) with increasing x values, signifying the progressive evolution of the lattice parameter within the cubic unit cell in the solid solution $Bi_{1.5}Nb_{1.5}Zn_xCu_{1-x}O_7$ and the effective incorporation of the dopant into the pyrochlore matrix.

Table 1:The lattice parameters, volumes, crystallite and grain size for Bi_{1.5}Nb_{1.5}Zn_xCu_{1-x}O₇ system, prepared by conventional solid state route.

| Contents of Zn(%) | 0 | 20 | 60 | 80 | 100 | |
|-------------------|---|----|----|----|-----|--|

Abba Malika.et.al Structural, Morphological, and Spectroscopic Study of Zn doped Bi_{1.5}Nb_{1.5}CuO₇ Pyrochlore Compounds

| a (Å) | | 10.5422 | 10.5481 | 10.5501 | 10.511 | 10.5587 |
|----------------------------|----------|---------|----------|---------|---------|---------|
| V (ų) | | 1171.65 | 1173.61 | 1174.27 | 1174.62 | 1177.16 |
| | Scherrer | 57.0067 | 109.6283 | 53.1112 | 52.7948 | 57.0126 |
| | (nm) | | | | | |
| Crystallite and grain size | SEM | 10.27 | 10.76 | 8.84 | 2.80 | 2.82 |
| | (µm) | | | | | |

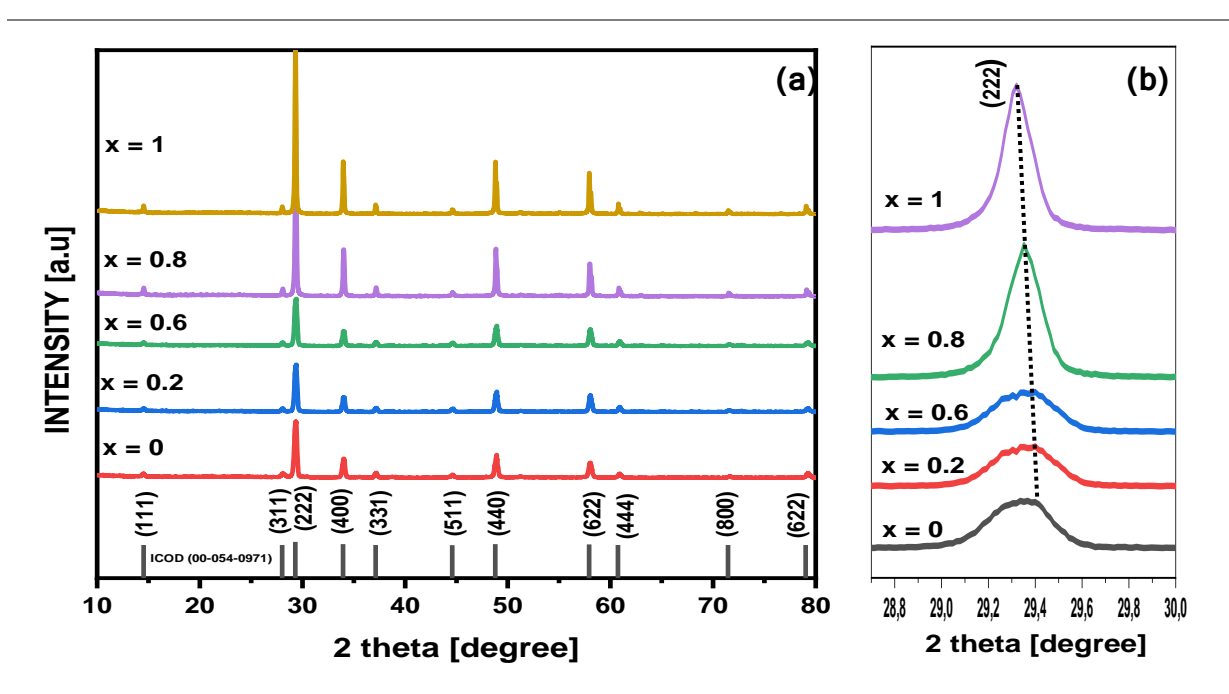


Fig. 3. (a) XRD Patterns of Bi_{1.5}Nb_{1.5}Zn_xCu_{1-x}O₇Ceramics Sintered at 920°C, with (b) Enlarged View (28.5° to 30°) Showing (222) Peak Position Evolution

The lattice parameters and corresponding volumes for the different compositions were refined using the Celref software (Table 1 and Fig. 4). The increase in lattice parameter is attributed to the difference in the ionic radii of zinc (0.74 Å) and copper (0.73 Å), both having a coordination number of VI[26, 27]. The substitution of copper with the larger zinc cation leads to an observed increase in lattice parameter. Additionally, X-ray diffraction analysis provided information on the average size of crystallites or coherence length, estimated using the Scherrer equation ($L = K \times \lambda / (\beta \times \cos(\theta))$), where L represents the average crystallite size. Within the solid solution $Bi_{1.5}Nb_{1.5}Zn_xCu_{1-x}O_7$, crystallite sizes were observed to vary between 110 and 52 nm (Table 1), corresponding to an increase in zinc concentration. This reduction in crystallite size is frequently correlated with enhanced crystallinity of the material, implying a more orderly structure as zinc is integrated[27, 28].

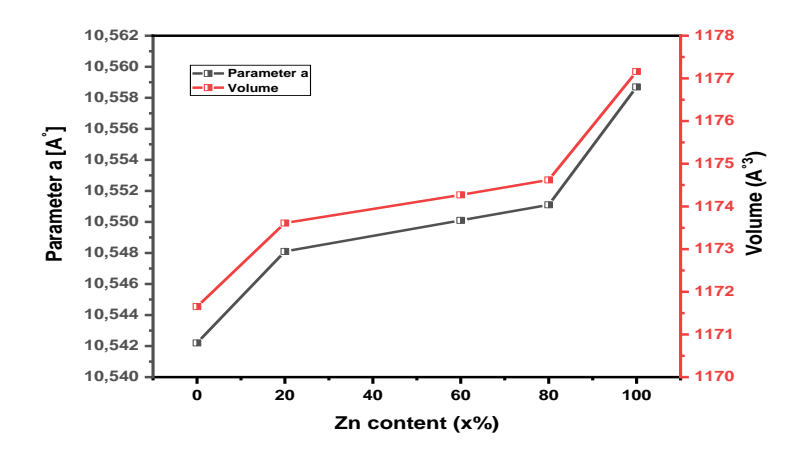


Fig. 4.Cell parameter and volume variation of the $Bi_{1.5}Nb_{1.5}Zn_xCu_{1-x}O_7$ ceramics sintered at 920°C (x = 0, 20, 60, 80 and 100%)

3.2. Density Measurements

The powders of the solid solution $Bi_{1.5}Nb_{1.5}Zn_xCu_{1-x}O_7$ doped with five different zinc concentrations (x = 0, 0.2, 0.6, 0.8, and 1) were used to form pellets with a diameter of Φ = 13 mm and a thickness of approximately e ≈ 1.5 mm. The results, including theoretical density, experimental density, and densification ratio of the sintered pellets after heating at 920°C for 12 hours, are presented in Table 2.

Table 2: The theoretical density, experimental density, and densification ratio of the Bi_{1.5}Nb_{1.5}Zn_xCu_{1-x}O₇ system sintered at 920°C.

| Sintering temperature (°C) | Contents of Zn(%) | Experimental density | Theoretical density | Densification ratio (%) |
|----------------------------|-------------------|----------------------|------------------------|-------------------------|
| | 0 | 6.5087 | 7.1235 | 91.3694 |
| | 20 | 6.5298 | 7.1157 | 91.1766 |
| 920 °C | 60 | 6.7502 | 7.1200 | 94.8061 |
| | 80 | 6.8297 | 7.1220 | 95.8958 |
| | 100 | 6.3751 | 7.1101 | 89.6625 |

Notably, the composition doped with 80% zinc exhibited the highest density value, measuring 6.8297 g/cm³, which corresponds to approximately 95.8958% of the theoretical density. This

increase in density indicates a reduction in the number and size of pores, resulting in a more compact structure. Enhanced compactness can be attributed to the densification process during sintering, where particles fuse and fill void spaces, resulting in a denser and more homogeneous material [29, 30].

3.3. Morphological Analysis via Scanning Electron Microscopy (SEM)

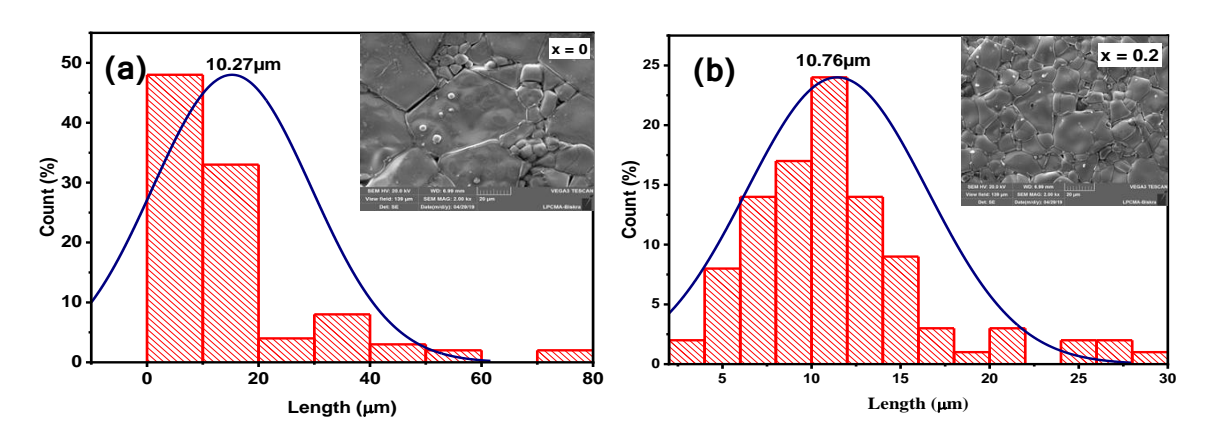
Fig. 5 (a- e) illustrate the grain size calculation curves conducted using « Image J » Software, and the corresponding micrographs of each composition were obtained through scanning electron microscopy (SEM). These analyses reveal that the compositions exhibit relatively larger grain sizes compared to the crystallite sizes calculated by the Debye-Scherrer method, ranging from $10.27~\mu m$ to $2.82~\mu m$, but these differences are correlated with experimental results and can be attributed to various factors, including densification effects, crystalline growth, and thermal treatment parameters [31].

3.4. Fourier Transform Infrared Spectroscopy (FTIR)

Fig. 5(f)presents the Infrared spectra of the $Bi_{1.5}Nb_{1.5}Zn_xCu_{1-x}O_7$ system. The observed vibrations in this spectral range are primarily associated with the metal-oxygen bonds. Notably, these spectra confirm the pyrochlore nature of the compounds within the system.

Variations in the relative intensity of specific bands are observed in response to changes in the substitution fraction, x. For instance, the bands located around 561 and 574 cm⁻¹ can be assigned to the polyhedron (Bi/[Zn Cu]) O_6O_2). These bands are situated within the region of stretching vibrations of the A-O and A-O bonds in the polyhedron AO_6O_2 , as explained by Withers et al [32].

It is noteworthy to mention that the absorption peaks at 1643 cm⁻¹ and 1372 cm⁻¹ can be ascribed to atmospheric CO₂, whereas the bands at approximately 3400 cm⁻¹ correspond to the stretching vibration of hydroxide (O-H) groups resulting from the presence of moisture[33, 34].



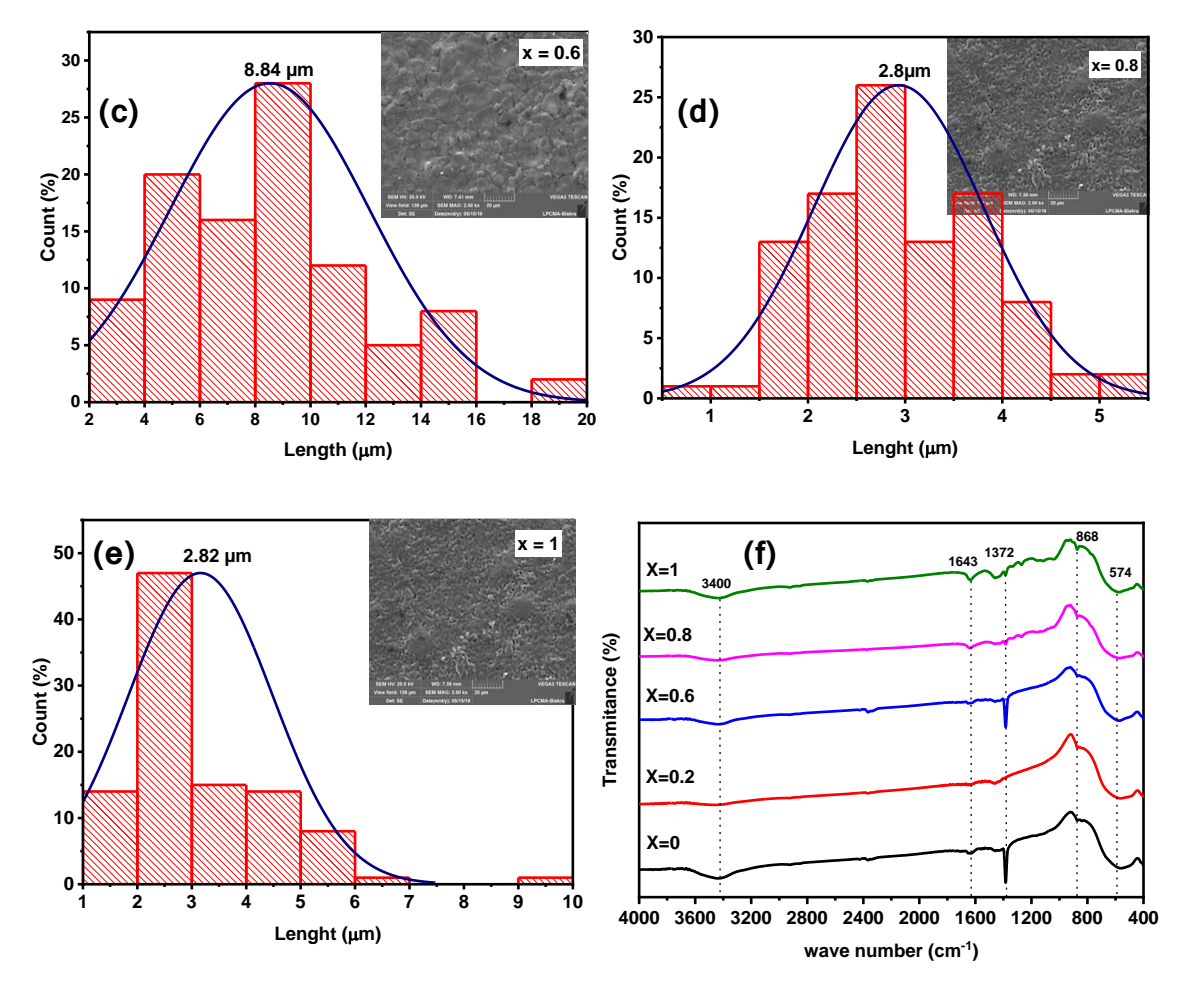


Fig.5. (a- e)SEM micrographs and the average grain sizes distribution with various contents of Zn, and (f)FTIR spectra of $Bi_{1.5}Nb_{1.5}Zn_xCu_{1-x}O_7$ (x = 0, 0.2, 0.6, 0.8 and 1)

3.5. UV-visible spectroscopy

UV-Visible spectroscopy, in conjunction with the Tauc Optical Characterization (TOC) plot, serves as a widely adopted analytical technique for determining the bandgap energy in semiconductor materials based on absorbance data[35]. The TOC plot, as depicted in Fig. 6(b), is generated from absorbance data recorded in the wavelength range of 200 to 800 nm, as shown in Fig. 6(a). The relationship between the material's absorbance (α), incident photon energy (hv), pre-exponential constant (A), bandgap energy (Eg), and an exponent (n) contingent upon the absorption mechanism is described by the equation (1)[19]:

$$(\alpha h v)^{n} = A(h v - Eg)$$
(1)

Typically, for an indirect transition, n = 1/2, while for a direct transition, n = 2.

By fitting a linear line to these data points, we can determine the bandgap energy, Eg, of the material. Using the indirect transition with an exponent 'n' of 1/2, our findings indicate that the

bandgap energy increases from 2.72 eV (x = 0) to 2.81 eV (x = 0.2), 2.91 eV (x = 0.6), 3.06 eV (x = 0.8), and 3.35 eV (x = 1) with an increasing zinc doping concentration. These results are in close agreement with the findings of Khiera, Zouaoui et al.[20].

Furthermore, our research reveals a significant correlation between the rising zinc doping concentration and a reduction in grain size of the samples. Generally, as grain size decreases, the quantum confinement effect leads to an increase in the bandgap energy, which aligns with our experimental data[36]. This variation in the bandgap energy with grain size has noteworthy implications for the optoelectronic and photocatalytic properties of these materials, rendering them particularly suitable for specific environmental applications.

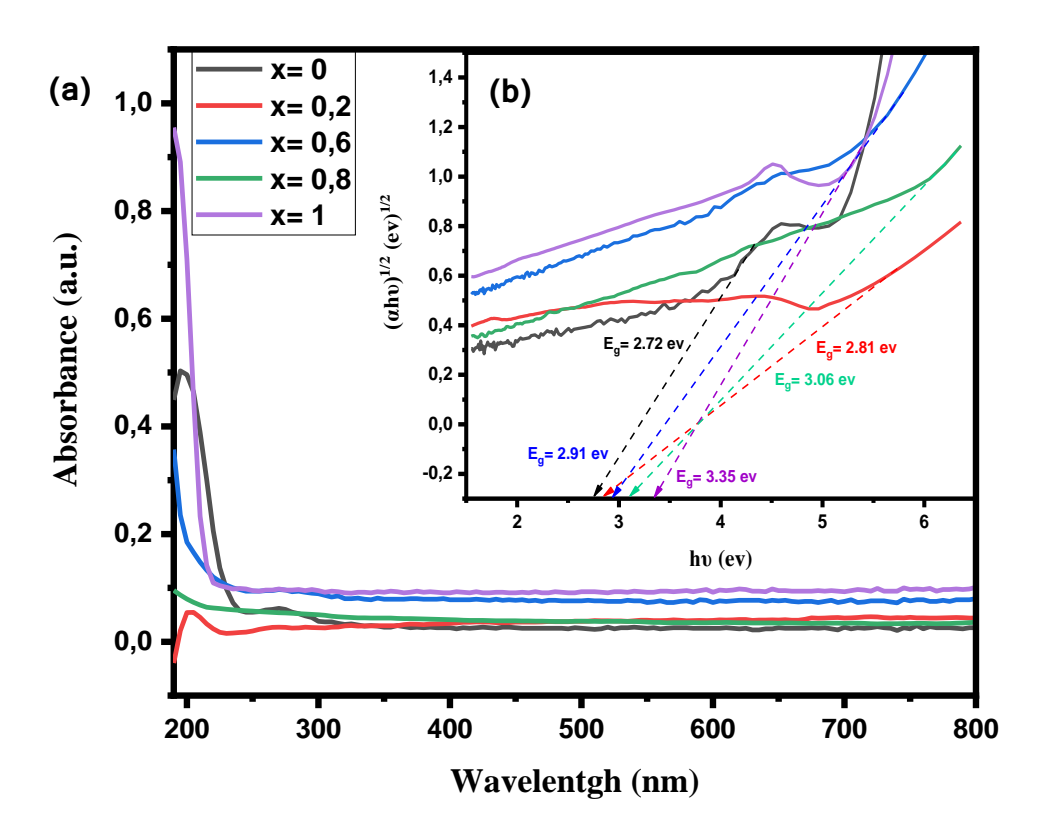


Fig. 6.(a) The UV–vis absorption (DRS) spectra and (b)Tauc plot of $Bi_{1.5}Nb_{1.5}Zn_xCu_{1-x}O_7$ where x=0,0.2,0.6,0.8, and 1.

4. Conclusion

The objective of this study was to synthesize and characterize pyrochlore-type solid solutions with the chemical formula $Bi_{1.5}Nb_{1.5}Zn_xCu_{1-x}O_7$ (x = 0, 0.2, 0.6, 0.8, and 1) using the solid-solid synthesis method. X-ray diffraction analysis revealed that all selected compositions exhibited a cubic structure with the Fd3m space group. Refinement of the lattice parameter "a" using Celref software demonstrated a continuous increase with the percentage of zinc doping. The average grain size, determined by the Scherrer method, ranged from 110 nm to 52 nm across different

compositions. Density and porosity studies of samples sintered at 920°C showed that the composition with 80% zinc doping achieved the highest density (6.8297 g/cm³) and the lowest porosity (4.1042%), indicating its superior properties. Infrared analysis (FTIR) conducted on samples sintered at 920°C revealed the presence of characteristic metal-oxygen bond vibrations in the range of 500 to 600 cm⁻¹, confirming the pyrochlore-type nature of the compounds. Scanning Electron Microscopy (SEM) images displayed an agglomerated structure with irregular distribution and uniform shapes. Furthermore, the optical bandgap, determined using the Tauc method, exhibited a low value in the copper composition, progressively increasing with the introduction of zinc. The bandgap values ranged from 2.72 eV to 3.35 eV.

These results demonstrate the successful synthesis and characterization of pyrochlore solid solutions with tunable properties, suggesting their potential as catalysts for environmental remediation.

References

- [1] Zhou, H., T.-J. Park, and S.S.J.J.o.m.r. Wong, Synthesis, characterization, and photocatalytic properties of pyrochlore Bi 2 Ti 2 O 7 nanotubes. 2006. 21: p. 2941-2947.
- [2] Li, N., Y. Yin, F. Meng, Q. Zhang, J. Yan, and Q.J.A.C. Jiang, Enabling pyrochlore-type oxides as highly efficient electrocatalysts for high-capacity and stable Na–O2 batteries: the synergy of electronic structure and morphology. 2017. 7(11): p. 7688-7694.
- [3] Ahuja, V., S. Baskar, and P.J.A.A.E.M. Senguttuvan, *Exploration of Pyrochlore-Bi2Sn2O7 as an Anode for Potassium-Ion Batteries*. 2023. **6**(7): p. 3665-3670.
- [4] Jitta, R.R., R. Gundeboina, N.K. Veldurthi, R. Guje, V.J.J.o.C.T. Muga, and Biotechnology, *Defect pyrochlore oxides: as photocatalyst materials for environmental and energy applications- a review.* 2015. **90**(11): p. 1937-1948.
- [5] Zeng, J., H. Wang, Y. Zhang, M.K. Zhu, and H.J.T.J.o.P.C.C. Yan, *Hydrothermal synthesis and photocatalytic properties of pyrochlore La2Sn2O7 nanocubes.* 2007. 111(32): p. 11879-11887.
- [6] Ogawa, M., H. Suzuki, O. Tomita, A. Nakada, R.J.J.o.P. Abe, and P.A. Chemistry, Sn2+-based pyrochlore oxysulfides with narrow band gaps for photocatalytic water splitting. 2023: p. 114895.
- [7] Supriya, S.J.C.C.R., Influence of rare earth coordinated elements in titanium-based pyrochlores and their dielectric phenomena. 2023. **493**: p. 215319.
- [8] Bailey, O., S. Husremovic, M. Murphy, J. Ross, J. Gong, D. Olds, and G.J.J.o.M.C.C. Laurita, Compositional influence of local and long-range polarity in the frustrated pyrochlore system Bi 2– x RE x Ti 2 O 7 (RE= Y 3+, Ho 3+). 2022. 10(37): p. 13886-13895.

- [9] Josserand, G., L. Chaffron, J. Ribis, P.-F. Giroux, T. Gloriant, and D.J.J.o.S.S.C. Simeone, X-ray diffraction study of oxygen deficient Y2Ti2O7- δ pyrochlore powders synthesized by high-energy ball milling (HEBM). 2022. 315: p. 123446.
- [10] Smerald, A. and G.J.P.R.L. Jackeli, Giant magnetoelastic-coupling driven spin-lattice liquid state in molybdate pyrochlores. 2019. 122(22): p. 227202.
- [11] Xin, Y., C. Xing, H. Zhou, and J. Liu, *Defects in Pyrochlore Dy2Ti2O7 Thin Film*, 2023, Oxford University Press US.
- [12] Gupta, S.K., M. Abdou, P.S. Ghosh, J.P. Zuniga, E. Manoharan, H. Kim, and Y.J.J.o.t.A.C.S. Mao, *On comparison of luminescence properties of La2Zr2O7 and La2Hf2O7 nanoparticles*. 2020. **103**(1): p. 235-248.
- [13] Luo, F., B. Li, Z. Guo, Y. Xie, L. Li, D. Shao, H. Zhang, X.J.M.C. Lu, and Physics, *Ab initio calculation of mechanical and thermodynamic properties of Gd2Zr2O7 pyrochlore.* 2020. **243**: p. 122565.
- [14] O'Sullivan, M., J. Alaria, M.S. Dyer, J.B. Claridge, M.W. Gaultois, and M.J.J.A.M. Rosseinsky, *Epitaxial growth, optical and electrical conductivity of the metallic pyrochlore Bi2Ru2O7 on Y-stabilized ZrO2 substrate.* 2023. 11(5).
- [15] Nekipelov, S.V., V.N. Sivkov, D.V. Sivkov, A.M. Lebedev, R.G. Chumakov, A.V. Koroleva, B.A. Makeev, and N.A.J.I. Zhuk, XPS and NEXAFS Studies of Zn-Doped Bismuth Iron Tantalate Pyrochlore. 2023. 11(7): p. 285.
- [16] Berri, S., K. Kaur, D. C Gupta, S.A. Sofi, J. Singh, M. Srinivasana, A.F. Wani, I.U.N.J.J.o.S. Lone, and N. Magnetism, *Tailoring the Inherent Magnetism and Thermoelectric Response of Pyrochlore Oxide A2B2O7 (A= Er, B= Ru, Sn, Ge, Pt): A Computational Approach.* 2023. 36(4): p. 1203-1215.
- [17] Matsumoto, A., Z.-X. Cai, and T.J.M. Fujita, Synthesis of Pyrochlore Oxides Containing Ir and Ru for Efficient Oxygen Evolution Reaction. 2022. 15(17): p. 6107.
- [18] Mandal, B.P. and A. Tyagi, *Ionic conductivity in materials with a pyrochlore structure*, in *Pyrochlore Ceramics*2022, Elsevier. p. 277-294.
- [19] Mayouf, S., C. Vincent, M. Fadia, Z. Kheira, T. Bouazza, and B.J.J.o.S.S.C. Naceur, Synthesis and characterization of a new ordered rhombohedral pyrochlore family Ln3Sb3Cu2O14 (Ln= Pr, Nd, Sm, Eu, Tb, Dy) with more detailed study of the Sm compound. 2023. 326: p. 124205.
- [20] Khiera, Z., T. Bouazza, B. Mohamed, S. Mayouf, and C.J.J.o.S.S.C. Vincent, *Synthesis, structural, optical and dielectric characterization of new pyrochlore solid solution B1.* 5Sb1. 5Zn1-xCuxO7. 2023. **321**: p. 123917.
- [21] Ellert, O.G. and A.V.J.P.C. Egorysheva, Unusual magnetic properties of ternary Bi-and Ln-containing pyrochlores: From cooperative paramagnetism to canted antiferromagnetism and reentrant spin glass. 2022: p. 315-338.

- [22] Naceur, B., E. Abdelkader, L. Nadjia, M. Sellami, and B. Noureddine, *Synthesis and characterization of Bi1.56Sb1.48Co0.96O7 pyrochlore sun-light-responsive photocatalyst.*Materials Research Bulletin, 2016. 74: p. 491-501 DOI: https://doi.org/10.1016/j.materresbull.2015.11.012.
- [23] Abdelbaky, M., A. Abdelghany, A. Oraby, E. Abdelrazek, and M.J.S.R. Rashad, Efficacious elimination of crystal violet pollutant via photo-Fenton process based on Gd (2- x) La (x) Zr2O7 nanoparticles. 2023. 13(1): p. 7723.
- [24] Wang, Z., C. Zhu, H. Wang, M. Wang, C. Liu, D. Yang, and Y.J.J.o.N.M. Li, Preparation and irradiation stability of A2B2O7 pyrochlore high-entropy ceramic for immobilization of high-level nuclear waste.2023. 574: p. 154212.
- [25] Korichi, H., Synthèse et caractérisation d'une nouvelle solution solide de type pyrochlore de formule Bi1. 5Nb1. 5Cu1-x ZnxO7: application catalytique, 2014, UNIVERSITE DES SCIENCES ET DE LA TECHNOLOGIE D'ORAN.
- [26] Menasra, H.J.T.R.S., Zinc-Ion Doped 7-Layer Aurivillius Compounds (Bi8. 75zn0. 25ti7o27): Structural, Morphological, and Optical Characterization. 2023: p. 5006-5016.
- [27] Labhane, P., V. Huse, L. Patle, A. Chaudhari, G.J.J.o.M.S. Sonawane, and C. Engineering, *Synthesis of Cu doped ZnO nanoparticles: crystallographic, optical, FTIR, morphological and photocatalytic study.* 2015. **3**(07): p. 39.
- [28] Esgin, H., Y. Caglar, M.J.J.o.A. Caglar, and Compounds, *Photovoltaic performance and physical characterization of Cu doped ZnO nanopowders as photoanode for DSSC.* 2022. **890**: p. 161848.
- [29] Qu, Z., C. Wan, and W.J.A.M. Pan, Thermophysical properties of rare-earth stannates: effect of pyrochlore structure. 2012. **60**(6-7): p. 2939-2949.
- [30] Michael, E.K. and S.J.J.o.t.A.C.S. Trolier-McKinstry, Cubic pyrochlore bismuth zinc niobate thin films for high-temperature dielectric energy storage. 2015. **98**(4): p. 1223-1229.
- [31] Joseph, D., C. Kaliyaperumal, S. Mumoorthy, and T.J.C.I. Paramasivam, *Dependence* on temperature of the electrical properties of nanocrystalline Y2Ti2O7 ceramics. 2018. 44(5): p. 5426-5432.
- [32] Withers, R., T. Welberry, A.-K. Larsson, Y. Liu, L. Norén, H. Rundlöf, and F.J.J.o.S.s.c. Brink, Local crystal chemistry, induced strain and short range order in the cubic pyrochlore (Bi1. 5– αZn0. 5– β)(Zn0. 5– γNb1. 5– δ) O (7– 1.5 α– β– γ– 2.5 δ)(BZN). 2004. 177(1): p. 231-244.
- [33] Stevens Jr, R.W., R.V. Siriwardane, J.J.E. Logan, and fuels, *In situ Fourier transform infrared (FTIR) investigation of CO2 adsorption onto zeolite materials.* 2008. **22**(5): p. 3070-3079.

Structural, Morphological, and Spectroscopic Study of Zn doped Bi_{1.5}Nb_{1.5}CuO₇ Pyrochlore Compounds

- [34] Garbout, A., S. Bouattour, A.B. do Rego, A. Ferraria, and A.J.J.o.c.g. Kolsi, *Synthesis, Raman and X-ray diffraction investigations of rubidium-doped Gd1. 8Ti2O6. 7 pyrochlore oxide via a sol–gel process.* 2007. **304**(2): p. 374-382.
- [35] Kurlla, P., A.K. Shivram, N. Kottam, S.B. Siddegowda, M. Subramaniam, U. Bogegowda, M. Subramanya, A.P. Chowdhury, R.L.J.E.S. Narasimhan, and P. Research, Green-engineered synthesis of Bi2Zr2O7 NPs: Excellent performance on electrochemical sensor and sunlight-driven photocatalytic studies. 2023: p. 1-21.
- [36] Movlarooy, T.J.M.R.E., Study of quantum confinement effects in ZnO nanostructures. 2018. 5(3): p. 035032.